ACS Photonics

Article

pubs.acs.org/journal/apchd5

Self-Assembled Layer (SAL)-Based Doping on Black Phosphorus (BP) Transistor and Photodetector

Dong-Ho Kang,[†,‡] Min Hwan Jeon,[§,‡] Sung Kyu Jang,[§] Woo-Young Choi,[†] Kyong Nam Kim,[∥] Jinok Kim,[†] Sungjoo Lee,[§] Geun Young Yeom,[*,§,⊥] and Jin-Hong Park[*,†,§]

[†]School of Electronic and Electrical Engineering, Sungkyunkwan University, Suwon 16419, Korea

[§]SKKU Advanced Institute of Nano Technology (SAINT), Sungkyunkwan University, Suwon 16419, Korea

[∥]School of Advanced Materials Science and Engineering, Daejeon University, Daejeon 330-716, Korea

[⊥]Department of Advanced Materials Science and Engineering, Sungkyunkwan University, Suwon 440-746, Korea

Supporting Information

ABSTRACT: Black phosphorus (BP) is appealing as a next-generation two-dimensional (2D) van der Waals (vdW) material, but research into doping BP to optimize device performance is still deficient. Here, we study n- and p-doping of variously thick (2, 4, 7, and 10 nm) black phosphorus (BP) films in terms of the performance of the corresponding BP-based transistors and photodetectors. N- and p-doping were respectively achieved with 3-amino-propyltriethoxysilane (APTES) and octadecyltrichlorosilane (OTS). The changed concentrations of BP were between approximately -2.1×10^{11} and -4.82×10^{11} cm^{-2} for APTES (n-doping) and between 1.06×10^{11} and 1.96×10^{11} cm^{-2} for OTS (p-doping). In the transistor devices formed on a 2 nm thick BP film, n-doping negatively shifted the threshold voltage from 28.3 to 19.5 V. Conversely, after p-doping with OTS, the threshold voltage was positively shifted from 20.6 to 23.7 V. In the BP photodetectors (2 nm thick devices), responsivity (R) was reduced by −16% (520 nm) and −9% (850 nm) after n-doping, whereas p-doping improved the responsivity by 40% (520 nm) and 20% (850 nm). Through this doping study, the very high photoresponsivity of 1.4×10^4 A/W under 520 nm laser exposure was achieved in 10 nm thick BP/OTS photodetectors. In addition, the n- and p-doping effects were more obvious in thin BP films.

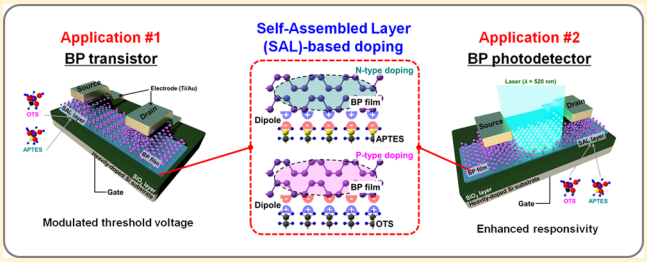

KEYWORDS: *black phosphorus, self-assembled layers, electronic device, optoelectronic device, OTS, APTES*

Black phosphorus (BP), which is a stable allotrope of phosphorus with a puckered two-dimensional (2D) layered structure, is considered a promising material that can be used to overcome the current limitations of two-dimensional (2D) van der Waals (vdW) materials (e.g., transition metal dichalcogenides (TMDs) and graphene). The mobility of bulk BP was theoretically predicted to be of the order of 10^4 $cm^2/(V{\cdot}s)$ by Akahama et al.[1] Li et al. reported a mobility of 10^3 $cm^2/(V{\cdot}s)$ in a BP field-effect transistor (FET) fabricated on few-layer-thick BP films,[2] demonstrating the potential for future fast-switching electronic devices. It was also reported that bulk BP retains its direct band gap properties, in contrast to other TMDs (e.g., molybdenum disulfide (MoS_2) and tungsten diselenide (WSe_2)), although its energy band gap is dependent on the number of BP layers (varying from 0.3 eV (bulk) to 2 eV (single-layer)).[3,4] Owing to its unique optical properties, BP is considered a suitable material for future 2D optoelectronic devices.[5−7] Buscema et al. recently demonstrated a wide-range spectral BP-based photodetector that exhibited high photoresponsivity to light from the infrared (997 nm) to the ultraviolet region (under 400 nm).[5] However, the relationship between the doping process and BP device performance has not been investigated in detail, in terms of the performance optimization of BP-based electronic/optoelectronic devices. For TMDs like MoS_2 and WSe_2, many doping techniques have previously been reported; doping has been carried out with potassium,[8] NO_2,[9] benzyl viologen,[10] self-assembled monolayers,[11,12] phosphorus silicate glass,[13] deoxyribonucleic acid (DNA),[14,15] thiol-based molecular chemisorption,[16] and Cs_2CO_3.[17] These doping techniques have led to performance enhancements in various TMD-based electronic/optoelectronic devices (e.g., increase in mobility and photoresponsivity) by reducing the metal-TMD contact resistance and carrier lifetime in the TMD region. Likewise, it is possible to optimize the performance of BP-based devices by applying doping techniques. Chen et al. recently reported the surface transfer doping phenomenon by Cs_2CO_3 and MoO_3 in BP-based devices; they also achieved high electron mobility (27 $cm^2/(V{\cdot}s)$) in 10 nm Cs_2CO_3-doped BP transistors and high photoresponsivity (2.56 A/W) in 8 nm MoO_3-doped BP photodetectors.[18]

Received: April 18, 2017
Published: June 20, 2017

DOI: 10.1021/acsphotonics.7b00398
ACS Photonics 2017, 4, 1822−1830

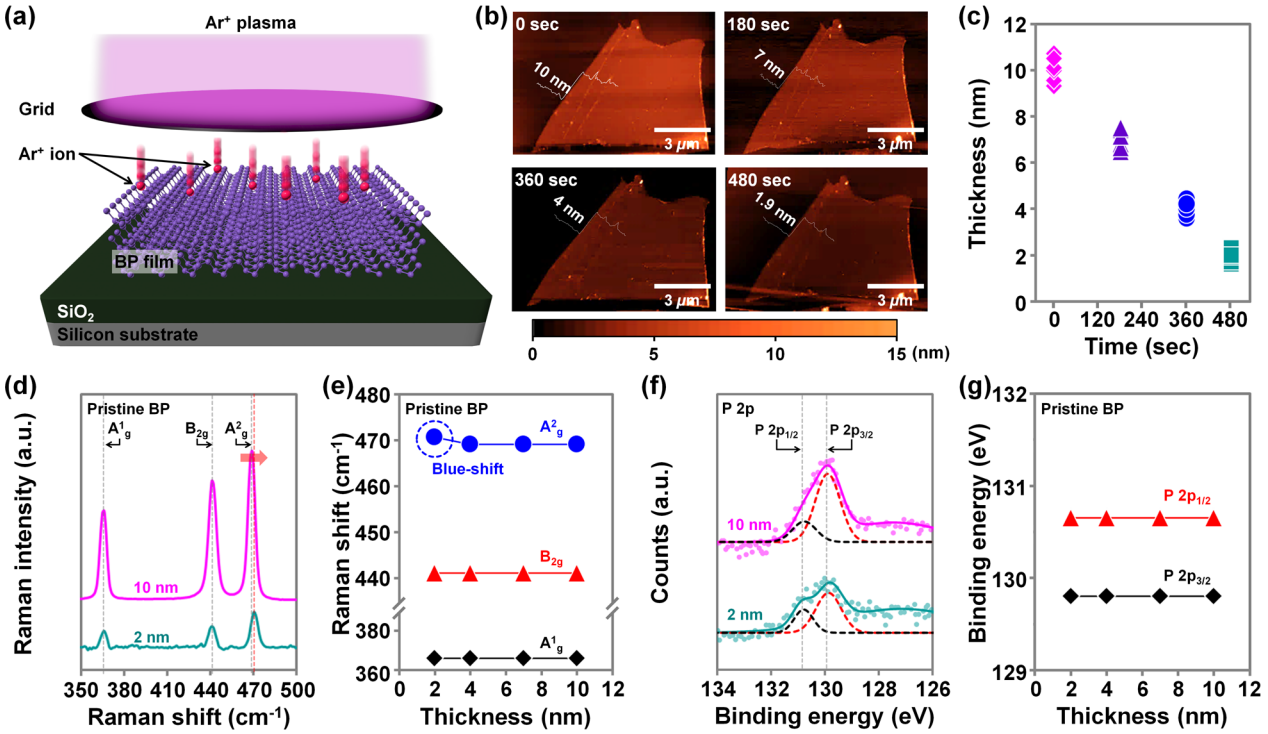

Figure 1. Characterization of BP films of various thicknesses. (a) Schematic illustration of Ar^+ plasma treatment process applied to the BP films. (b) AFM images of thinned BP films with various plasma treatment processing times (0, 180, 360, and 480 s). (c) The plasma-etched BP flake thickness as a function of the plasma treatment processing time. (d) Raman spectra of 2 nm and 10 nm thick BP films and (e) extracted Raman peak positions of BP films as a function of BP thickness. (f) XPS analysis of 2 nm and 10 nm thick BP films with binding energy peaks of P $2p_{3/2}$ and $2p_{1/2}$ and (g) spin−orbital P 2p core peaks of BP films as a function of BP thickness.

Here, we study n- and p-type doping phenomena in BP transistor and photodetector devices with various BP thicknesses (2, 4, 7, and 10 nm), which are respectively based on the dipole formations of self-assembled layers (SALs) such as 3-amino-propyltriethoxysilane (APTES) and octadecyl-trichlorosilane (OTS). The functional groups in APTES (NH_3-) and OTS (CH_3-) have negative and positive charges, respectively, which are able to adjust the carrier density in the BP channel. In the first part of this study, we investigate APTES- and OTS-doping at different thicknesses of BP by Raman spectroscopy and X-ray photoelectron spectroscopy. The film thickness was modulated by a low-energy ion beam thinning process. The effects of doping on the various parameters of electronic devices (V_{TH}, carrier concentration, and on-current) are discussed by analyzing the electrical data (I_D-V_G and I_D-V_D). Finally, we analyze the APTES- and OTS-doping effects in terms of the photoresponsivity of BP photodetectors under exposure to lasers with various wavelengths (520, 655, 785, and 850 nm).

RESULTS AND DISCUSSION

Characterization of Plasma-Etched BP Films. First, we prepared few-layer-thick BP films by mechanical exfoliation onto SiO_2/Si substrates using Scotch tape. This was followed by low-power Ar^+ plasma treatment to obtain BP films of varying thicknesses (2, 4, 7, and 10 nm). Figure 1a shows a schematic illustration of the few-layer-thick BP etching process. As Ar^+ ions move vertically in the Ar^+ ion beam system to cause ion bombardment on the BP surface, Ar^+ ions can break P−P bonds in the BP top layer when their energy is higher than the P−P bonding energy. However, if Ar^+ ions have excess energy, a large portion of the energy is transferred to the bottom layer, which can severely damage the BP structure. Therefore, we found suitable process conditions to minimize the structural damage on the BP layer (see the Experimental Methods and Supporting Information, Figure S1). The etched BP films were analyzed using atomic force spectroscopy (AFM), Raman spectroscopy, and X-ray photoelectron spectroscopy (XPS). Figure 1b,c shows the AFM images and thicknesses of BP flims obtained after the plasma-etching. The thickness of the BP flims was reduced from 10 to 7 nm after plasma treatment for 180 s; this was subsequently reduced to 4 and 1.9 nm after 360 and 480 s, respectively. Next, we extracted the thickness data at six different points (on the same BP flake) to verify the uniformity of the plasma etching process and to estimate the etch rate. In Figure 1c, the extracted thicknesses of the BP flims were uniformly distributed around the average value at all conditions (approximately ±1 nm from the average value) and the etch rate was calculated to be approximately 1 nm/min. Figure 1d,e shows the results of Raman spectroscopy analysis performed on BP flims with various thicknesses. The Raman spectra show three conventional peaks in 10 nm and 2 nm thick BP flims; these peaks appeared at 366.16 cm^{-1} (A^1_g peak), 441.1 cm^{-1} (B_{2g} peak), and 469.11 cm^{-1} (A^2_g peak). The A^1_g peak of BP indicates the out-of-plane vibration mode, and the other two peaks (B_{2g} and A^2_g) correspond to the in-plane vibration modes.[19] Figure 1e shows that the A^2_g peak was blue-shifted by $\Delta = 1.64$ cm^{-1} in the 2 nm thick BP film, while the other peaks (A^1_g and B_{2g}) did not change as a function of thickness. This blue-shift of the A^2_g peak in the 2 nm thick sample seems to be related to the interlayer van der Waals forces in BP. According to Wan et al.,[20] blue-shift of the BP Raman peak with decreasing thickness is caused by acceleration of the oscillation

DOI: 10.1021/acsphotonics.7b00398
ACS Photonics 2017, 4, 1822−1830

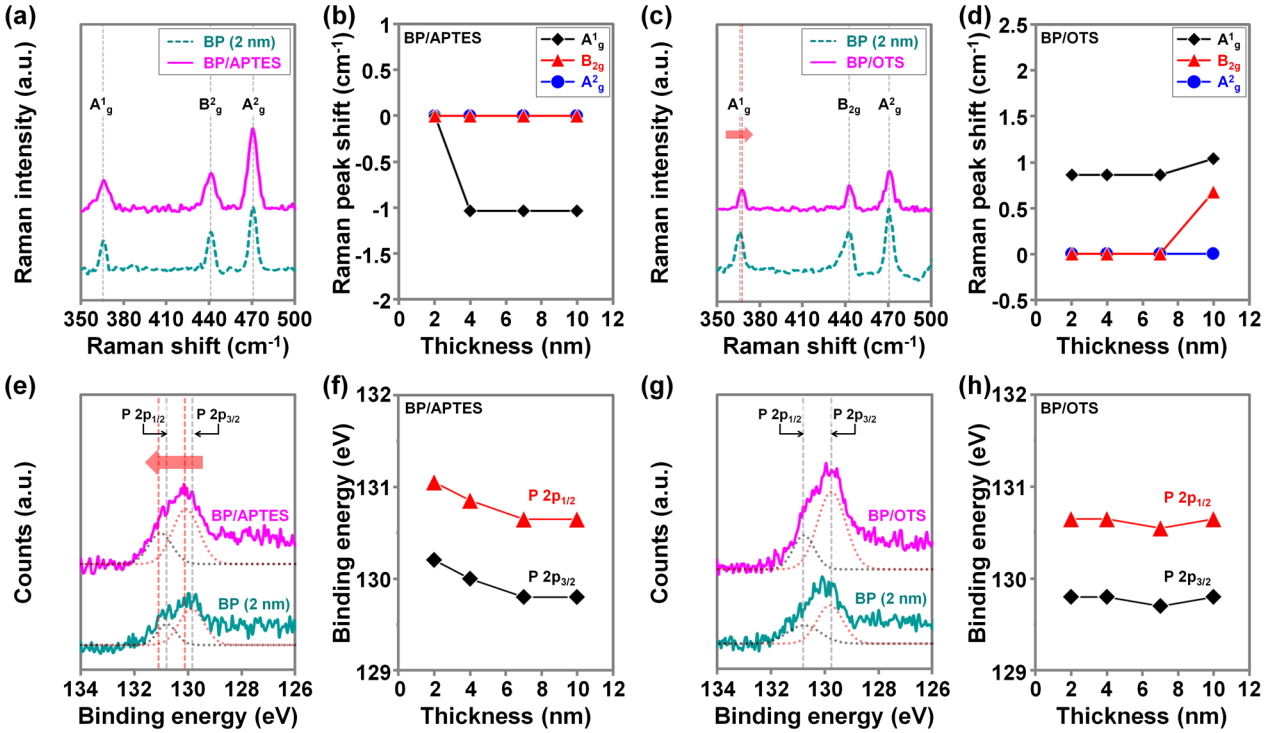

Figure 2. Characterization of BP films of various thicknesses before/after APTES- and OTS-doping. Raman spectra of 2 nm thick BP films before/after (a) APTES- and (c) OTS-doping. Extracted Raman peak shift values of BP films after (b) APTES and (d) OTS doping as a function of the BP film thickness. XPS analysis of 2 nm thick BP before and after (e) APTES- and (g) OTS-doping with binding energy peaks of P $2p_{3/2}$ and $2p_{1/2}$ electrons. Spin−orbital P 2p core peaks of (f) APTES- and (h) OTS-doped BP films as a function of BP thickness.

in P atoms that occurred owing to weakening of the van der Waals forces between BP layers.

To investigate the structural damage of plasma-etched BP films, we performed XPS analysis on the variously thick BP films. In Figure 1f, we observed spin−orbital P 2p core peaks ($2p_{3/2}$ and $2p_{1/2}$ at 129.8 and 130.65 eV, respectively) in both the 2 nm and 10 nm thick BP films. This suggests that the BP structure consisted of only P−P bonding and did not undergo any damage because of chemical reactions (e.g., native oxidation or hydroxylation). In addition, we confirmed that the positions of the P $2p_{3/2}$ and P $2p_{1/2}$ peaks were independent of the thickness of the BP film (Figure 1g). If the BP films had experienced structural damage during the etching process, the binding energy of the P−P bonds would be modulated by chemical reactions with oxygen or moisture in the air, which would result in up- or down-shifting of the XPS phosphorus peak position. Further, by investigating the root mean squared (RMS) values of each thinned BP film (Supporting Information, Figure S2), we also confirmed that there was very little damage caused to the BP surface during etching. The oxidized phosphorus peak, which observed at 135.05 eV in the as-exfoliated BP flakes, disappeared in the plasma-treated BP films (Supporting Information, Figure S3). Based on this result, it is predicted that our plasma etching process effectively removed the oxidized BP layer from the BP surface.

Raman Spectroscopy and XPS Analysis of SAL-Doped BP Films. To investigate the SAL-based doping of BP, we performed Raman spectroscopy and XPS analysis on BP films that were exfoliated on APTES- and OTS-treated SiO_2/Si substrates. The thickness of the BP film was adjusted from 10 to 2 nm by plasma etching. The concentration of APTES and OTS solutions was fixed at 1% (a detailed process is explained in the Experimental Methods). Figure 2a,c shows the Raman spectra that were obtained from APTES- and OTS-doped 2 nm thick BP films, respectively. These data were compared with those collected from undoped BP flakes of the same thickness. In Figure 2a (showing Raman spectra of 2 nm thick BP film), we did not observe any peak position changes (A^1_g, B_{2g}, and A^2_g) before and after APTES-doping. However, in BP films with different thicknesses (4, 7, and 10 nm), we found that the A^1_g peak was red-shifted ($\Delta = -1.04$ cm^{-1}) by APTES doping (see Figure 2b). It is thought that the concentration of electrons increased by the n-doping process softened the BP in-plane vibrational mode, subsequently causing the A^1_g peak to red shift. Alternatively, we confirmed blue-shifting of the A^1_g peak in the OTS-doped 2 nm thick BP film relative to the undoped sample, as shown in Figure 2c. This blue shift between 0.86 and 1.04 cm^{-1} was observed for all thicknesses of the OTS-doped BP films (Figure 2d). In addition, a smaller blue shift of the B_{2g} peak ($\Delta = 0.68$ cm^{-1}) was shown in the 10 nm thick BP film. The blue shifts of the B_{2g} and A^2_g Raman peaks seem to be induced by variations in the hole concentration varied by p-doping stiffened the BP in-plane vibration modes.[12]

We also performed XPS analysis to investigate the chemical binding of BP films with various thicknesses (2, 4, 7, and 10 nm) doped with APTES and OTS. Figure 2e and g present the XPS spectra of 2 nm thick BP films before/after APTES and OTS doping, respectively. The spin−orbital XPS peaks were up-shifted from 129.8 to 130.1 eV ($2p_{3/2}$) and from 130.65 to 130.95 eV ($2p_{1/2}$) in the APTES-doped BP film (Figure 2e), indicating that the Fermi level of BP moved toward the conduction band edge after APTES-doping (i.e., an n-type doping effect). Fang et al.[8] previously reported upshift of the XPS peaks of MoS_2 and WSe_2 after doping with potassium (n-doping), where the XPS peak shift values ranged between 0.6 and 0.8 cm^{-1} for MoS_2 and were approximately 0.4 cm^{-1} for

DOI: 10.1021/acsphotonics.7b00398
ACS Photonics 2017, 4, 1822−1830

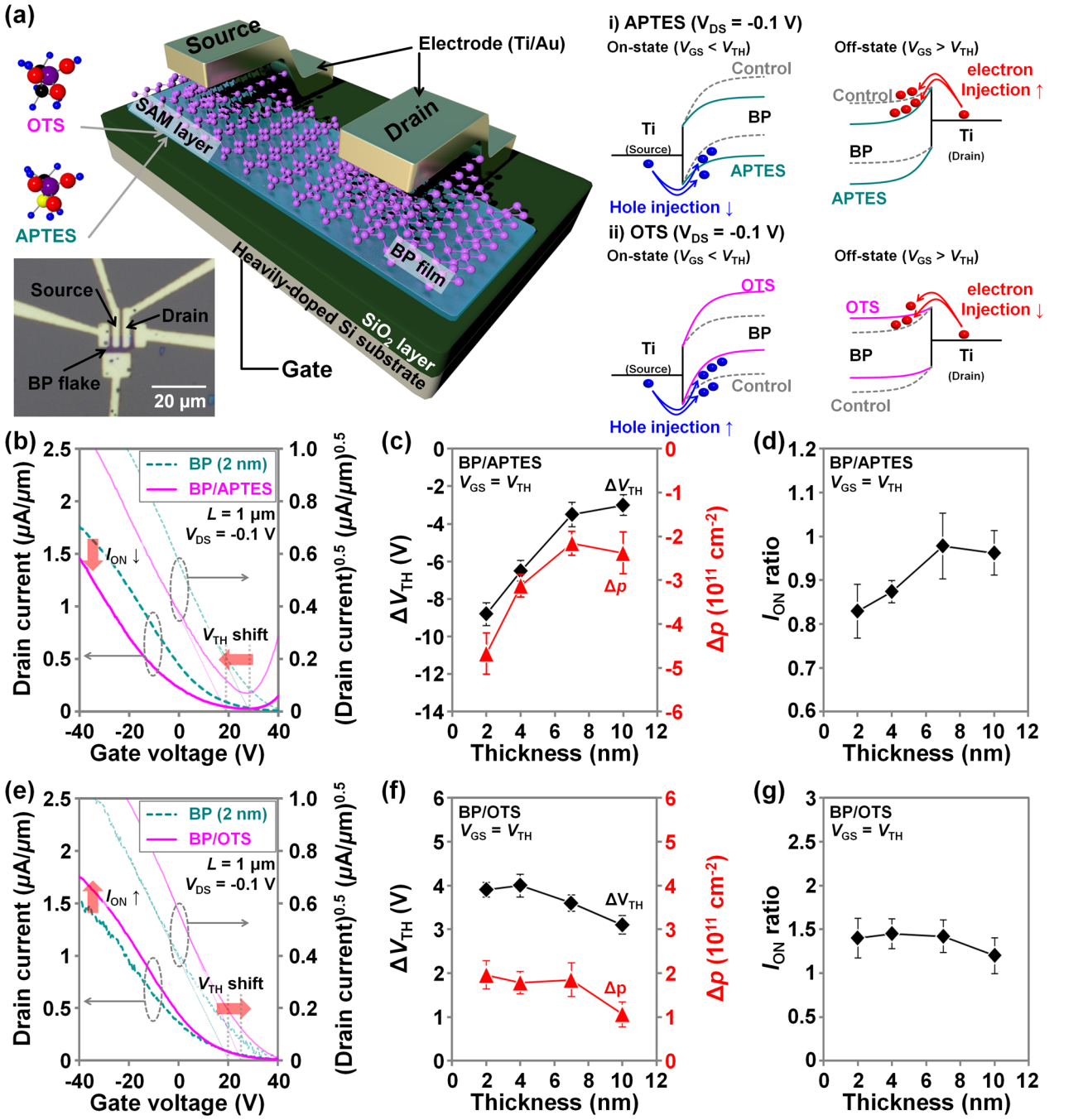

Figure 3. Electrical characterization of APTES- and OTS-doped BP transistors. (a) Schematic illustration/optical image of BP transistor devices doped by APTES and OTS and the energy band diagrams of Ti-BP-Ti junctions before/after (*i*) APTES and (*ii*) OTS doping. I_D–V_G and $I_D^{0.5}$–V_G characteristics of BP transistors before/after (b) APTES and (e) OTS doping. The extracted threshold voltage shifts ($\Delta V_{TH} = V_{TH\_SAL} - V_{TH\_control}$) and carrier concentration differences ($\Delta p = p_{\_SAL} - p_{\_control}$) at $V_{GS} = V_{TH}$ in the BP transistors after (c) APTES and (f) OTS doping. The on-current ratio (I_{ON} ratio = $I_{ON\_SAL}/I_{ON\_control}$) at $V_{GS} = -40$ V in BP transistors with (f) APTES and (g) OTS doping. Electrical parameters in absolute values as presented in the Supporting Information, Figure S5.

WSe_2. We then extracted the XPS peak position (binding energy) of each APTES-doped BP film with reducing thickness and plotted these values as a function of BP film thickness in Figure 2f. Compared to the XPS peak positions of the undoped BP film of the same thickness (129.8 eV for $2p_{3/2}$ and 130.65 eV for $2p_{1/2}$ at all BP thicknesses), peak-shifting was not observed in the 10 nm thick APTES-doped BP sample. However, as the BP film thickness decreased from 7 to 2 nm, we observed an increase in the peak position (binding energy) values from 0.1 to 0.3 eV for both the $2p_{3/2}$ and $2p_{1/2}$ peaks. This is because the intrinsic carrier concentration of BP film decreases with reducing thickness and this causes a relatively greater reduction in the concentration of holes by the same n-doping process (a more detailed explanation is in Figure 3). Alternatively, in Figure 2g, we observed no peak change in the 2 nm thick BP films after OTS-doping (p-doping). We also plotted the peak position values extracted in OTS-doped BP films by adjusting the film thickness from 10 to 2 nm (Figure 2h), where no relationship between the XPS peak position and the BP film thickness was observed. It is thought that the OTS-

DOI: 10.1021/acsphotonics.7b00398
ACS Photonics 2017, 4, 1822–1830

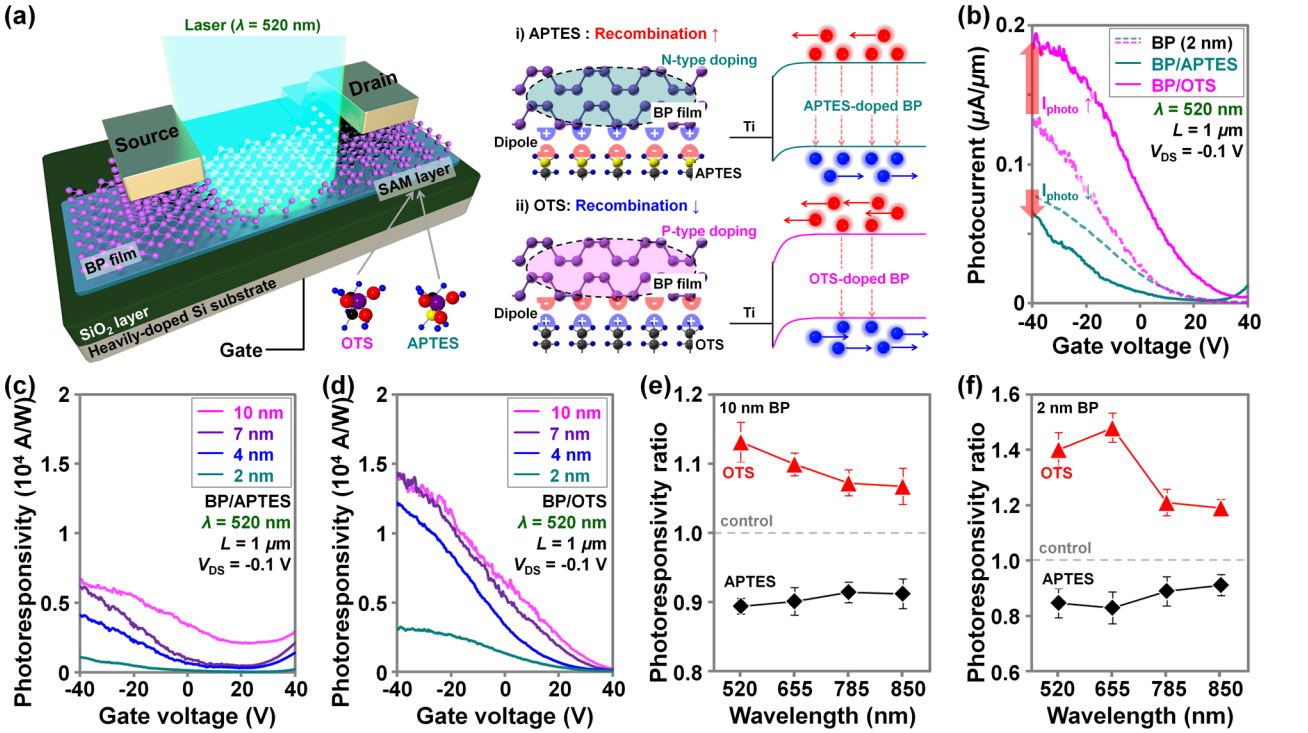

Figure 4. Optical characterization of APTES- and OTS-doped BP-based photodetectors. (a) Schematic illustration of SAL-doped BP photodetector under laser illumination (P_{light} = 6 mW/cm^2) and descriptive diagram showing the changes of photocarrier recombination in (*i*) APTES- and (*ii*) OTS-doped BP films. (b) I_{photo}–V_G characteristics of the undoped (dotted line) and APTES (pink solid line)/OTS (green solid line)-doped BP photodetectors. Photoresponsivity extracted from (c) APTES- and (d) OTS-doped BP photodetectors with various thicknesses (2, 4, 7, and 10 nm) as a function of the applied gate voltage. The photoresponsivity ratio ($R_{SAL}/R_{control}$) values as a function of the laser wavelength, which were extracted from APTES- and OTS-doped (e) 2 nm- and (f) 10 nm-thick BP photodetectors. Photoresponsivity in absolute values as presented in the Supporting Information, Figure S7.

doping effect is weaker than the APTES-doping effect in BP films that initially present strong p-doping property;[21] therefore, the XPS peak-shift caused by OTS-doping appears to be below the binding energy resolution of XPS (approximately 0.05 eV). In particular, for both APTES- and OTS-doping, a constant interval of approximately 0.85 eV was observed between the two peak positions ($2p_{3/2}$ and $2p_{1/2}$) regardless of the thickness of the BP film (refer to Figure 2f,h). This is because the two components of the XPS phosphorus peak, located at the same 2p core level, were simultaneously up- or down-shifted by SAL-based doping.

Electrical Characteristics of APTES- and OTS-Doped BP Transistors. To reconfirm the SAL-doping effects on BP, we fabricated back-gate BP transistors and performed current–voltage measurements on the resultant devices (I_D–V_G and I_D–V_D) before/after doping. Figure 3a shows the schematic illustration, the optical image of SAL-doped BP transistor, and the energy band diagrams of Ti-BP junctions before/after (*i*) n-doping (APTES) and (*ii*) p-doping (OTS). In the case of the APTES-doped BP transistor, the negative charges of the APTES functional groups down-shift the BP energy band, thereby reducing the electric field at the source-BP junction. This phenomenon decreases the tunneling probability of holes and subsequently increases the contact resistance between the source and BP channel. In addition, APTES-doping increases the electric field at the drain-BP junction and reduces the effective electron barrier height via barrier lowering, which eventually allows more electrons to be injected from the drain to the BP channel. As a result, APTES-doping on the BP transistor is expected to decrease hole conduction (on-current) and increase electron conduction (off-current). Chen et al. recently reported ambipolar behavior in BP transistors after light Cs_2CO_3-doping (n-doping, nondegenerate level) and also showed BP n-FETs with heavy Cs_2CO_3-doping (n-doping, degenerate level).[18] OTS-doping causes an upshift of the BP energy band owing to the positive charges of the OTS functional groups, consequently reducing the effective hole barrier height at the source-BP junction. As a result, the hole injection probability from the source into the BP channel also appears to increase, which enhances the on-current of BP transistors. Conversely, effective electron barrier height at the drain-BP junction increases after OTS-doping because the electric field at the junction is reduced by up-shifting of the energy band (i.e., no electron injection from the drain to the BP). Here, we only considered hole injection (source-BP junction) and electron injection (drain-BP junction) at the on- and off-state of BP transistors, respectively, because BP transistors operate in accumulation mode. To support this analysis, we performed transmission line method (TLM) measurements on the doped BP films and extracted the contact resistance, as shown in Figure S4. When OTS was coated on the BP devices, the contact resistance decreased from 108 kΩ·μm to 65 kΩ·μm. On the other hand, the contact resistance increased from 108 kΩ·μm to 186 kΩ·μm in the APTES-doped BP device. As expected, this result indicated that the OTS and APTES layers could improve/deteriorate carrier injection from the source to the BP by tuning the effective barrier height of metal-BP junctions.

We also performed electrical measurements on the APTES- and OTS-doped BP transistors and extracted various electrical

DOI: 10.1021/acsphotonics.7b00398
ACS Photonics 2017, 4, 1822–1830

parameters (ΔV_{TH}, Δp, and I_{on}). The 2D sheet doping concentration was calculated from $p = I_D L/qW\mu V_D$, where q is the electron charge, L and W are the length and width of the channel, respectively (both are 1 μm), and μ is the mobility. All carrier concentration values were normalized by the number of BP layers. Figure 3b,e shows the I_D-V_G characteristic curves of the 2 nm thick BP-based transistors before/after APTES and OTS doping. In this experiment, we used eight control samples that had similar electrical performances (on-current and V_{TH}). Four samples with on-current close to 1.5×10^{-6} A/μm at V_G = −40 V were used for the OTS experiment, and four other samples with on-current close to 1.75×10^{-6} A/μm were used for the APTES experiment. Because of this experimental design, the $I-V$ curves of the control samples presented in Figure 3b,e are slightly different. As shown in Figure 3b, the on-current level (at V_{GS} = −40 V) decreased from 1.76×10^{-6} A/μm to 1.46×10^{-6} A/μm and the threshold voltage was negatively shifted from 28.3 to 19.5 V (ΔV_{TH} = −8.8 V) after APTES-doping (n-doping). We plotted the electrical parameters as a function of BP film thickness (between 10 and 2 nm). In Figure 3c, when the BP thickness was reduced from 10 to 2 nm, the ΔV_{TH} and Δp values decreased from −2.8 to −8.8 V and from -2.1×10^{11} to -4.82×10^{11} cm^{-2}, respectively. In addition, the on-current ratio ($I_{ON\_SAL}/I_{ON\_control}$) decreased from 0.97 to 0.83 as the BP film thickness decreased (Figure 3d). This decreasing trend indicates that the APTES-doping phenomenon becomes more pronounced for thinner BP channels; this observation is consistent with our XPS analysis (refer to Figure 2f). Alternatively, for OTS-doping (Figure 3e), the on-current increased from 1.54×10^{-6} to 1.76×10^{-6} A/μm and the threshold voltage was positively shifted from 20.6 to 23.7 V. Thinning the BP films from 10 to 2 nm increased the ΔV_{TH} and Δp values from 3.1 to 3.9 V and from 1.06×10^{11} to 1.96×10^{11} cm^{-2}, respectively. The on-current ratio increased from 1.15 (10 nm) to 1.4 (2 nm), also indicating that the OTS doping effect becomes more pronounced for thinner BP films; this is similar to the case of APTES doping. The SAL doping concentrations (-4.82×10^{11} and 1.96×10^{11} cm^{-2} for n- and p-doping, respectively) are lower than those of other BP doping techniques using Cs_2CO_3 (1.5×10^{12} cm^{-2}, n-doping),[18] MoO_3 (6.0×10^{12} cm^{-2}, p-doping),[18] and 1-ethyl-3-methylimidazolium bis(trifluoromethanesulfonyl)imide (>10^{13} cm^{-2}, p-doping).[22] We also investigated SAL doping effects on 150 nm thick BP devices (Supporting Information, Figure S8), where we could not observe any variations in V_{TH} and on-current. These results are thought to be attributed to the intrinsic carrier concentration (n_i) difference of the BP channels, which is dependent on the BP film thickness. Typically, the intrinsic carrier concentration of bulk BP films is higher than that of few-layer-thick BP films because bulk BP has a vdW structure in which several BP monolayers are stacked (the carrier density of monolayer BP is approximately 10^{13} cm^{-2} at 300 K[23]). Thus, SAL doping that is able to induce the same concentration of carriers has a greater influence on thinner BP films with lower intrinsic carrier concentration, resulting in larger variations in V_{TH} and on-current.

Optical Characteristics of SAL-Doped BP Photodetectors. To further examine the SAL-based doping effects in terms of photodetector device performance, we carried out typical I_D-V_G measurements with BP-based photodetectors upon exposure to various wavelengths (λ = 520, 655, 785, and 850 nm) of lasers. A three-dimensional schematic illustration of the SAL-doped BP photodetector and graphical explanations describing photocarrier recombination in (*i*) APTES- and (*ii*) OTS-doped BP films are shown in Figure 4a. In the case of APTES doping, we expect that the number of electrons in BP increased because of the negative polarity of the NH_2-functional groups in the APTES, which increases the density of unstable excitons and charged excitons; these excitons easily dissociate and recombine with each other. Therefore, the photocurrent deterioration caused by APTES doping seems to originate from the increase in recombination probability in BP. In Figure 4b, we plotted the photocurrent (when exposed to a 520 nm laser) as a function of the gate voltage before/after APTES doping. Compared to the control device, the photocurrent of the APTES-doped BP photodetector decreased from 77.9 to 65.9 nA/μm. Conversely, for OTS-doping, the recombination rate of photocarriers appears to be reduced in the BP channel. It is thought that the CH_3- functional groups in OTS hold electrons in BP,[24] reducing the density of unstable and charged excitons. As a result, the photocurrent increased from 133 to 187 nA/μm after OTS doping (Figure 4b). A similar phenomenon was reported in WSe_2 photodetectors after OTS doping (p-doping), where the photoresponsivity values were improved by a factor of 28.2; this phenomenon was due to the decreased recombination rate of negatively charged trions by p-doping.[12] Then, to evaluate the SAL-doped BP photodetectors in detail, we calculated photoresponsivity values from the I_D-V_G curves of the photodetectors with various BP thicknesses (10, 7, 4, and 2 nm) using $R = I_{photo}/P_{light}$, where I_{photo} is the photocurrent ($I_{laser\_on} - I_{laser\_off}$) and P_{light} is the incident power of the laser source. The photoresponsivity data was plotted as a function of the gate voltage bias in Figure 4c,d. The photoresponsivities showed an increasing trend as reducing the gate bias (V_{GS}) to −40 V due to the increase in BP channel conductivity. In addition, the photoresponsivity tended to decrease as the BP film thickness was reduced in both APTES- and OTS-doped devices. The maximum photoresponsivity values (at V_{GS} = −40 V) of the APTES- and OTS-doped BP photodetectors decreased from 6.7×10^3 (10 nm) to 1.1×10^3 A/W (2 nm) and from 1.4×10^4 (10 nm) to 3.11×10^3 A/W (2 nm), respectively. The interfacial scattering effect between the BP channel and the gate dielectric (or at the plasma-etched surface) seemed to intensify when the BP channel was thinned, decreasing the photoresponsivity. Here, the maximum photoresponsivity value (1.4×10^4 A/W) is higher than that of other BP and TMD-based photodetectors that were recently reported in the literature (100 A/W on BP,[25] 8.16×10^2 A/W on MoS_2,[26] 4.2×10^2 A/W on WSe_2,[27] 4×10^3 A/W on ReS_2,[28] and 8×10^2 A/W on $ReSe_2$[29]). For a fair comparison, we used the responsivity values under similar wavelength (500−532 nm) and incident power (5−10 nW). Finally, we extracted the maximum photoresponsivity values of the undoped and SAL-doped BP devices under exposure to lasers of four different wavelengths (520, 655, 785, and 850 nm) to minutely investigate the SAL-doping effects in terms of the spectral response of the BP photodetector. Figure 4e,f presents the photoresponsivity ratio ($R_{SAL}/R_{control}$) of the SAL-doped 10 and 2 nm BP photodetectors, respectively, as a function of the laser wavelength (520, 655, 785, and 850 nm). The deterioration and improvement of the photoresponsivity caused by doping with APTES and OTS, respectively, occurred at all wavelengths (R ratio: 0.82−0.92 in BP/APTES and 1.08−1.49 in BP/OTS samples). In addition, when lower wavelength lasers (below 655 nm) were irradiated on the SAL-doped BP photodetectors, the photoresponsivity ratio varied slightly more

DOI: 10.1021/acsphotonics.7b00398
ACS Photonics 2017, 4, 1822−1830

(Figures 4e and f). This phenomenon is expected to originate from the wavelength-dependent absorption properties of BP films. In general, BP films show higher absorption under exposure to lasers with lower wavelengths,[30] which can increase the number of photocarriers in the BP photodetectors. For a reference, the wavelength-dependence of photoresponsivity was also reported in MoS_2- and WSe_2-based photodetectors, where the photoresponsivity ratios under exposure to 520 and 655 nm lasers (R ratio: 13−17.2) were higher than the values under exposure to 785 and 850 nm lasers (R ratio: 1.5−2).[12]

CONCLUSIONS

We investigated n-doping and p-doping by APTES and OTS, respectively, on BP films with different thicknesses (2, 4, 7, and 10 nm). Characterization of the doping effects was completed with Raman spectroscopy, XPS analysis, and electrical and optical measurements. The changes in 2D doping concentrations of BP films varied between -2.1×10^{11} and -4.82×10^{11} cm^{-2} for APTES and between 1.06×10^{11} and 1.96×10^{11} cm^{-2} for OTS while reducing the BP film thickness. Through Raman and XPS analyses, we found that SAL-doping only affected the A^1_g peak (the in-plane vibrational mode) of BP. We also observed an increase in the spin−orbital XPS ($2p_{3/2}$ and $2p_{1/2}$) peak positions (binding energies) from 0.1 to 0.3 eV as the BP film thickness was reduced from 7 to 2 nm. Additionally, we studied the SAL-doping effects on the performance of BP devices with varying film thicknesses. In the transistors formed on 2 nm thick BP films, n-doping negatively shifted the threshold voltage from 28.3 to 19.5 V. The degree of negative V_{TH} shift increased from −2.8 to −8.8 V as the BP films thinned from 10 to 2 nm. Conversely, after p-doping with OTS, the threshold voltage positively shifted from 20.6 to 23.7 V, and this positive V_{TH} shift value increased as the BP film thickness decreased (ΔV_{TH}: 3.1 → 3.9 V). In the BP photodetectors (2 nm thick devices), photoresponsivity (R) reduced by −16% (520 nm) and −9% (850 nm) after n-doping, whereas p-doping improved the photoresponsivity by 40% (520 nm) and 20% (850 nm). In addition, the n- and p-doping effects were stronger in thin BP photodetectors (n-doping: −16% (2 nm) > −8% (10 nm); and p-doping: 40% (2 nm) > 24% (10 nm)). Through this doping study, a high photoresponsivity (1.4×10^4 A/W at 520 nm) was achieved in 10 nm thick BP/OTS photodetectors, which was higher than that of state-of-the-art TMD photodetectors. In current research on BP devices, the crucial factors that restrict the BP device performance are (*i*) environmental instability of BP film due to high affinity with H_2O/O_2 molecules in air and (*ii*) a narrow bandgap of few-layer/bulk BP film (0.3 eV) that causes a low on-/off-current ratio and high dark current. To further improve BP device performance, it is essential to develop techniques for obtaining a monolayer BP film (E_g = 2.0 eV) that is completely isolated from air.

EXPERIMENTAL METHODS

Formation of APTES- and OTS-Doped BP Samples. To form APTES and OTS layers on SiO_2 layers (285 nm thick) grown on a heavily doped p-type Si substrate (resistivity < 0.005 Ω·m), 500 μL of OTS (≥90%, Sigma-Aldrich) and APTES (99%, Sigma-Aldrich) were added to 50 mL of hexane (a mixture of isomers, ≥99%, Sigma-Aldrich) and toluene (99.8%, Sigma-Aldrich), respectively. SiO_2/Si substrates were soaked in each solution for 1 h. After treatment, the samples were rinsed with toluene, alcohol, and deionized water and baked at 120 °C for 20 min in a vacuum oven to remove the remaining solvents. BP flakes were mechanically exfoliated onto the APTES- and OTS-doped SiO_2/Si substrates with blue Nitto tape (Supporting Information, Figure S9).

Obtaining and Verifying the Fabrication of BP Thin Films. BP thin films were obtained by Ar^+ plasma treatment. The detailed fabrication system is presented in the Supporting Information (Figure S1). Here, the first, second, and third grid voltages were 30, −150, and 0 V, respectively. The ICP source power and process pressure were 200 W and 3.5 mTorr, respectively. The thickness and surface roughness of undoped, APTES-doped, and OTS-doped BP samples were investigated by performing atomic force microscopy (AFM) at room temperature. The heights of all BP flakes were measured using 300 kHz Si cantilevers in the normal tapping mode. AFM images were obtained using 256 samples per line at a scanning rate of 0.5 Hz. The local surface roughness was measured over an area of 2 μm × 2 μm and roughness values were determined by analyzing the root mean squared (RMS) roughness.

Characterization of APTES- and OTS-Doped BP Films. APTES- and OTS-doped BP samples were investigated and compared with a control sample using PL/Raman spectroscopy (Alpha300 M+, WITec) and X-ray photoelectron spectroscopy (ESCA2000, VG Microtech Inc.). A Raman spectroscope with an excitation wavelength of 532 nm was used. The laser beam size was 0.7−0.9 μm and the instrumental spectral resolution was below 0.6 cm^{-1}. A Mg Kα twin-anode source with an X-ray incident angle of 0° was used for the XPS measurements.

Fabrication of APTES- and OTS-Doped BP Devices. To fabricate back-gated BP devices, we transferred BP films to the APTES- and OTS-treated SiO_2/Si substrates and performed Ar^+ plasma thinning on the films for 10 min. We then used e-beam lithography to pattern the source/drain electrodes (channel length and width = 1 μm). This was followed by the deposition of Ti (10 nm) and Au (50 nm) via an e-beam evaporator. After fabricating the BP devices, we repeated Ar^+ plasma thinning to adjust the thickness of the BP film. Next, poly(methyl methacrylate) (PMMA) was coated onto the BP devices to prevent chemical reaction and oxidation of the BP films by O_2 and H_2O in the air.

Electrical and Optical Characterization of APTES- and OTS-Doped BP Devices. The fabricated devices were analyzed by taking electrical measurements (I_D-V_G and I_D-V_D) with an HP 4155A semiconductor parameter analyzer with/without exposure to lasers with various wavelengths. The threshold voltage (V_{TH}) and carrier concentration (p) were calculated from the measured data. Here, all drain currents (I_D) were normalized by the channel width (W). The 2D carrier concentration was extracted using n (or p) = $I_D L/qW\mu V_D$, where L and W are the length and width of the channel, respectively, q is the electron charge, and μ is the mobility. The light source was a dot laser with wavelengths of 520, 655, 785, and 850 nm and an optical power of 0.6 mW/cm^2. The photoresponsivity (R) was extracted from $R = I_{photo}/P_{light}$, where I_{photo} is the generated photocurrent and P_{light} is the total incident optical power. After performing all electrical and optical measurements in the APTES- and OTS-doped BP devices, we transferred the BP devices onto the pristine SiO_2/Si substrates through a wet transfer technique (pristine BP device). Then, we repeated the electrical/optical measurements with the pristine BP device.

DOI: 10.1021/acsphotonics.7b00398
ACS Photonics 2017, 4, 1822−1830

■ ASSOCIATED CONTENT

Supporting Information

The Supporting Information is available free of charge on the ACS Publications website at DOI: 10.1021/acsphotonics.7b00398.

The ion beam thinning system used to obtain thin black phosphorus flakes; Root mean squared (RMS) values of thinned BP films; XPS analysis performed on as-exfoliated and pre-etched BP films; Contact resistance extraction on the control and OTS- and APTES-doped BP devices; Threshold voltage and on-current values of the control, APTES-doped, and OTS-doped BP transistors; Electrical characteristics (I_D−V_G of pristine, APTES-doped, and OTS-doped BP transistors with various BP thicknesses; Photoresponsivity values of the control and APTES- and OTS-doped BP photodetectors with various film thicknesses (2 and 10 nm); APTES doping effect on a 150 nm thick BP device; Fabrication process flow for SAL-doped BP transistor and photodetector devices; Investigation of PMMA encapsulation effects on BP transistors (PDF).

■ AUTHOR INFORMATION

Corresponding Authors

*E-mail: jhpark9@skku.edu.

*E-mail: gyyeom@skku.edu.

ORCID

Sungjoo Lee: 0000-0003-1284-3593

Geun Young Yeom: 0000-0001-7516-8404

Jin-Hong Park: 0000-0001-8401-6920

Author Contributions

‡D.-H.K. and M.H.J. contributed equally to this work.

Notes

The authors declare no competing financial interest.

■ ACKNOWLEDGMENTS

This research was supported by the Basic Science Research Program, Basic Research Lab Program and Nano·Material Technology Development Program through National Research Foundation of Korea (NRF) grants funded by the Korea government (MSIP) (NRF 2015R1A2A2A01002965, 2015M3A7B7045496, 2017R1A4A1015400, 2016M3A7B4910426, and 2016M3A7B4910429), and the Future Semiconductor Device Technology Development Program (10067739) funded by Ministry of Trade, Industry & Energy (MOTIE) and Korea Semiconductor Research Consortium (KSRC).

■ REFERENCES

(1) Akahama, Y.; Endo, S.; Narita, S. Electrical Properties of Black Phosphorus Single Crystals. *J. Phys. Soc. Jpn.* **1983**, *52*, 2148−2155.

(2) Li, L.; Yu, Y.; Ye, G. J.; Ge, Q.; Ou, X.; Wu, H.; Feng, D.; Chen, X. H.; Zhang, Y. Black Phosphorus Field-Effect Transistors. *Nat. Nanotechnol.* **2014**, *9*, 372−377.

(3) Tran, V.; Soklaski, R.; Liang, Y.; Yang, L. Layer-Controlled Band Gap and Anisotropic Excitons in Few-Layer Black Phosphorus. *Phys. Rev. B: Condens. Matter Mater. Phys.* **2014**, *89*, 235319.

(4) Qiao, J.; Kong, X.; Hu, Z.-X.; Yang, F.; Ji, W. High-Mobility Transport Anisotropy and Linear Dichroism in Few-Layer Black Phosphorus. *Nat. Commun.* **2014**, *5*, 4475.

(5) Buscema, M.; Groenendijk, D. J.; Blanter, S. I.; Steele, G. A.; Zant, H. S. J. v.; Gomez, A. C. Fast and Broadband Photoresponse of Few-Layer Black Phosphorus Field-Effect Transistors. *Nano Lett.* **2014**, *14*, 3347−3352.

(6) Engel, M.; Steiner, M.; Avouris, P. Black Phosphorus Photodetector for Multispectral, High-Resolution Imaging. *Nano Lett.* **2014**, *14*, 6414−6417.

(7) Youngblood, N.; Chen, C.; Koester, S. J.; Li, M. Waveguide-Integrated Black Phosphorus Photodetector with High Responsivity and Low Dark Current. *Nat. Photonics* **2015**, *9*, 247−252.

(8) Fang, H.; Tosun, M.; Seol, G.; Chang, T. C.; Takei, K.; Guo, J.; Javey, A. Degenerate n-Doping of Few-Layer Transition Metal Dichalcogenides by Potassium. *Nano Lett.* **2013**, *13*, 1991−1995.

(9) Fang, H.; Chuang, S.; Chang, T. C.; Takei, K.; Takahashi, T.; Javey, A. High-Performance Single Layered WSe_2 p-FET with Chemically Doped Contacts. *Nano Lett.* **2012**, *12*, 3788−3792.

(10) Kiriya, D.; Tosun, M.; Zhao, P.; Kang, J. S.; Javey, A. Air-Stable Surface Charge Transfer Doping of MoS_2 by Benzyl Viologen. *J. Am. Chem. Soc.* **2014**, *136*, 7853−7856.

(11) Kang, D.-H.; Shim, J.; Jang, S. K.; Jeon, J.; Jeon, M. H.; Yeom, G. Y.; Jung, W.-S.; Jang, Y. H.; Lee, S.; Park, J.-H. Controllable Nondegenerate p-Type Doping of Tungsten Diselenide by Octadecyltrichlorosilane. *ACS Nano* **2015**, *9*, 1099−1107.

(12) Li, Y.; Xu, C.-Y.; Hu, P.; Zhen, L. Carrier Control of MoS_2 Nanoflakes by Functional Self-Assembled Monolayer. *ACS Nano* **2013**, *7*, 7795−7804.

(13) Park, H.-Y.; Lim, M.-H.; Jeon, J.; Yoo, G.; Kang, D.-H.; Jang, S. K.; Jeon, M. H.; Lee, Y.; Cho, J. H.; Yeom, G. Y.; Jung, W.-S.; Lee, J.; Park, S.; Lee, S.; Park, J.-H. Wide-Range Controllable n-Doping of Molybdenum Disulfide (MoS_2) Through Thermal and Optical Activation. *ACS Nano* **2015**, *9*, 2368−2376.

(14) Park, H.-Y.; Dugasani, S. R.; Kang, D.-H.; Jeon, J.; Jang, S. K.; Lee, S.; Roh, Y.; Park, S. H.; Park, J.-H. n- and p-Type Doping Phenomenon by Artifical DNA and M-DNA on Two-Dimensional Transition Metal Dichalcogenides. *ACS Nano* **2014**, *8*, 11603−11613.

(15) Kang, D.-H.; Dugasani, S. R.; Park, H.-Y.; Shim, J.; Gnapareddy, B.; Jeon, J.; Lee, S.; Roh, Y.; Park, S. H.; Park, J.-H. Ultra-Low Doping on Two-Dimensional Transition Metal Dichalcogenides using DNA Nanostructure Doped by a Combination of Lanthanide and Metal Ions. *Sci. Rep.* **2016**, *6*, 20333.

(16) Sim, D. M.; Kim, M.; Yim, S.; Choi, M.-J.; Choi, J.; Yoo, S.; Jung, Y. S. Controlled Doping of Vacancy-Containing Few-Layer MoS_2 *via* Highly Stable Thiol-Based Molecular Chemisorption. *ACS Nano* **2015**, *9*, 12115−12123.

(17) Lin, J. D.; Han, C.; Wang, F.; Wang, R.; Xiang, D.; Qin, S.; Zhang, X.-A.; Wang, L.; Zhang, H.; Wee, A. T. S.; Chen, W. Electron-Doping-Enhanced Trion Formation in Monolayer Molybdenum Disulfide Functionalized with Cesium Carbonate. *ACS Nano* **2014**, *8*, 5323−5329.

(18) Xiang, D.; Han, C.; Wu, J.; Zhong, S.; Liu, Y.; Lin, J.; Zhang, X.-A.; Hu, W. P.; Özyilmaz, B.; Castro Neto, A. H.; Wee, A. T. S.; Chen, W. Surface Transfer Doping Induced Effective Modulation on Ambipolar Characteristics of Few-Layer Black Phosphorus. *Nat. Commun.* **2015**, *6*, 6485.

(19) Wang, X.; Jones, A. M.; Seyler, K. L.; Tran, V.; Jia, Y.; Zhao, H.; Wang, H.; Yang, L.; Xu, X.; Xia, F. Highly Anisotropic and Robust Excitons in Monolayer Black Phosphorus. *Nat. Nanotechnol.* **2015**, *10*, 517−521.

(20) Feng, Y.; Zhou, J.; Du, Y.; Miao, F.; Duan, C.-G.; Wang, B.; Wan, X. Raman Spectra of Few-Layer Phosphorene Studied From First-Principles Calculations. *J. Phys.: Condens. Matter* **2015**, *27*, 185302.

(21) Flores, E.; Ares, J. R.; Castellanos-Gomez, A.; Barawi, M.; Ferrer, I. J. Thermoelectric Power of Bulk Black-Phosphorus. *Appl. Phys. Lett.* **2015**, *106*, 022102.

(22) Jia, J.; Xu, J.; Park, J.-H.; Lee, B. H.; Hwang, E.; Lee, S. Multifunctional Homogeneous Lateral Black Phosphorus Junction Devices. *Chem. Mater.* **2017**, *29*, 3143−3151.

(23) Rudenko, A. N.; Brener, S.; Katsnelson, M. I. Intrinsic Charge Carrier Mobility in Single-Layer Black Phosphorus. *Phys. Rev. Lett.* **2016**, *116*, 246401.

DOI: 10.1021/acsphotonics.7b00398
ACS Photonics 2017, 4, 1822−1830

(24) Najmaei, S.; Zou, X.; Er, D.; Li, J.; Jin, Z.; Gao, W.; Zhang, Q.; Park, S.; Ge, L.; Lei, S.; Kono, J.; Shenoy, V. B.; Yakobson, B. I.; George, A.; Ajayan, P. M.; Lou, J. Tailoring The Physical Properties of Molybdenum Disulfide Monolayers by Control of Interfacial Chemistry. *Nano Lett.* **2014**, *14*, 1354−1361.
(25) Guo, Q.; Pospischil, A.; Bhuiyan, M.; Jiang, H.; Tian, H.; Farmer, D.; Deng, B.; Li, C.; Han, S.-J.; Wang, H.; Xia, Q.; Ma, T.-P.; Mueller, T.; Xia, F. Black Phosphorus Mid-Infrared Photodetectors with High Gain. *Nano Lett.* **2016**, *16*, 4648−4655.
(26) Zhang, W.; Huang, J.-K.; Chen, C.-H.; Chang, Y.-H.; Cheng, Y.-J.; Li, L.-J. High-Gain Phototransistors Based on a CVD MoS_2 Monolayer. *Adv. Mater.* **2013**, *25*, 3456−3461.
(27) Pradhan, N. R.; Ludwig, J.; Lu, Z.; Rhodes, D.; Bishop, M. M.; Thirunavukkuarasu, K.; McGill, S. A.; Smirnov, D.; Balicas, L. High Photoresponsivity and Short Photoresponse Times in Few-Layered WSe_2 Transistors. *ACS Appl. Mater. Interfaces* **2015**, *7*, 12080−12088.
(28) Shim, J.; Oh, A.; Kang, D.-H.; Oh, S.; Jang, S. K.; Jeon, J.; Jeon, M. H.; Kim, M.; Choi, C.; Lee, J.; Lee, S.; Yeom, G. Y.; Song, Y. J.; Park, J.-H. High Performance Two-Dimensional Rhenium Disulfide (ReS_2) Transistors and Photodetectors by Oxygen Plasma Treatment. *Adv. Mater.* **2016**, *28*, 6985−6992.
(29) Jo, S.-H.; Park, H.-Y.; Kang, D.-H.; Shim, J.; Jeon, J.; Choi, S.; Kim, M.; Park, Y.; Lee, J.; Song, Y.; Lee, S.; Park, J.-H. Broad Detection Range Rhenium Diselenide Photodetector Enhanced by (3-Aminopropyl)Triethoxysilane and Triphenylphosphine Treatment. *Adv. Mater.* **2016**, *28*, 6711−6718.
(30) Wang, H.; Yang, X.; Shao, W.; Chen, S.; Xie, J.; Zhang, X.; Wang, J.; Xie, Y. Ultrathin Black Phosphorus Nanosheets for Efficient Singlet Oxygen Generation. *J. Am. Chem. Soc.* **2015**, *137*, 11376−11382.

DOI: 10.1021/acsphotonics.7b00398
ACS Photonics 2017, 4, 1822−1830